A comparison of OH nightglow volume emission rates as measured by SCIAMACHY and SABER

Yajun Zhu[1, 2], Martin Kaufmann[1, 3], Qiuyu Chen[1, 3], Jiyao Xu[2, 4], Qiucheng Gong[1, 3], Jilin Liu[1, 3], Daikang Wei[1, 3], and Martin Riese[1, 3]

[1]Institute of Energy and Climate Research, Forschungszentrum Jülich, Jülich, Germany
[2]State Key Laboratory of Space Weather, National Space Science Center, Chinese Academy of Sciences, Beijing, China
[3]Institute for Atmospheric and Environmental Research, University of Wuppertal, Germany
[4]School of Astronomy and Space Science, University of Chinese Academy of Sciences, Beijing, China

Correspondence: Qiuyu Chen (q.chen@fz-juelich.de)

Abstract. Hydroxyl (OH) short-wave infrared emissions measured by the SCanning Imaging Absorption spectroMeter for Atmospheric CHartographY (SCIAMACHY) were used in this study to simulate OH 1.6 μm and 2.0 μm radiances as measured by the Sounding of the Atmosphere using Broadband Emission Radiometry (SABER) instrument. This paper presents a retrieval model to perform an inversion of OH(v) number densities in order to simulate OH ro-vibrational emission radiances using a non-linear regularized global fit technique. OH 1.6 μm and 2.0 μm radiances as measured by SABER were retrieved from OH limb measurements recorded by SCIAMACHY channel 6 for altitudes in the range of 80-96 km. The main source of uncertainty in the retrieval is related to the Einstein coefficients. Systematic deviations of up to 88% were found between SABER OH 1.6 μm and 2.0 μm radiance measurements and the corresponding simulations obtained from SCIAMACHY OH data. The radiometric calibration of the instruments could potentially explain the differences between the two measurements.

1 Introduction

Hydroxyl (OH) airglow stems from spontaneous emissions of metastable excited OH molecules which are mainly produced by the exothermic reaction of H and O_3 in the upper mesosphere and lower thermosphere (UMLT). Its emission layer peaks at an altitude approx. 87 km and extends about 8 km in thickness (Baker and Stair, 1988; Gao et al., 2010). OH airglow covers a broad spectral region from ultraviolet to near-infrared and is of importance for studying photochemistry and dynamics in the UMLT.

Since first confirmed by Meinel (1950) in the UMLT, OH airglow emissions have been widely observed using various remote spectroscopic techniques (e.g., Offermann and Gerndt, 1990; von Savigny et al., 2004; Kaufmann et al., 2008; Smith et al., 2010; Zhu et al., 2012). The measurements obtained in such studies have been analyzed for various purposes. For example, rotational temperature can be obtained from OH emissions as a proxy for kinetic temperature under the assumption of rotational

local thermodynamic equilibrium (LTE) (Offermann et al., 2010; Zhu et al., 2012; Liu et al., 2015). Gravity waves passing through the OH airglow layer can be captured to study the dynamics and energy balance in the UMLT (Xu et al., 2015). The understanding of OH relaxation mechanisms with different species can be improved by studying different OH band emissions in the UMLT (Kaufmann et al., 2008; Xu et al., 2012; von Savigny et al., 2012). Another important application of OH airglow

25 is to derive trace constituents in the UMLT, such as H and O abundances (Kaufmann et al., 2013; Mlynczak et al., 2018; Panka et al., 2018; Zhu and Kaufmann, 2018).

OH nightglow has been globally measured by two satellite instruments, SABER (Sounding of the Atmosphere using Broadband Emission Radiometry) operating since 2002, and SCIAMACHY (SCanning Imaging Absorption spectroMeter for Atmospheric CHartographY) observing from 2002 to 2012. SABER performed observations successfully over a 17-year period,

30 covering almost two solar cycles; many outstanding achievements have been accomplished (e.g., Xu et al., 2007; Smith et al., 2008; Mlynczak et al., 2010; Gao et al., 2010). The OH data obtained by SABER have been used by different investigators (Smith et al., 2010; Mlynczak et al., 2013; Panka et al., 2018; Mlynczak et al., 2018) to derive atomic oxygen abundance in the UMLT; however, deviations of up to 60% were found in comparison with atomic oxygen data derived from $O(^1S)$ green-line measurements obtained by SCIAMACHY and WINDII (Wind Imaging Interferometer) (Kaufmann et al., 2014; Zhu et al.,

35 2015). This large deviation promoted a discussion on the absolute values of atomic oxygen abundance (Mlynczak et al., 2018; Panka et al., 2018; Zhu and Kaufmann, 2018). Mlynczak et al. (2018) derived new atomic oxygen data from SABER OH 2.0 μm absolute radiance measurements in the UMLT under the constraints of the global annual mean energy budget. Panka et al. (2018) also retrieved atomic oxygen data from SABER OH 1.6 μm and 2.0 μm radiance ratios as an alternative approach. Further new atomic oxygen data were recently derived by Zhu and Kaufmann (2018) from SCIAMACHY nighttime OH(9-6) band

40 measurements using rate constants measured in the laboratory by Kalogerakis et al. (2016), which agree with atomic oxygen data derived from SCIAMACHY $O(^1S)$ green-line and O_2 A-band measurements within a range of 10-20% (Zhu and Kaufmann, 2019). While the agreement between new atomic oxygen data obtained by SABER and SCIAMACHY has improved, systematic deviations of up to 50% still persist (Zhu and Kaufmann, 2018). This systematic difference needs to be addressed in future studies. Here, we compare measured SABER OH 1.6 and 2.0 μm volume emission rates with corresponding simulated

45 values based on SCIAMACHY OH nighttime limb spectral measurements.

In this study, OH nightglow limb spectra measured by SCIAMACHY were used to derive OH absolute volume radiances. The retrieved absolute values were compared to SABER OH radiance measurements to investigate whether systematic differences exist between the two datasets.

2 OH nightglow measurements and auxiliary data

50 From 2002 to 2012, OH Meinel-band near-infrared emissions were measured simultaneously by SCIAMACHY on the Envisat and by SABER on the TIMED (Thermosphere, Ionosphere, Mesosphere Energetics and Dynamics) satellite. The spectral range of both instruments covers several OH emission bands stemming from different vibrational states (Kaufmann et al., 2008; Mlynczak et al., 2013). The SCIAMACHY instrument on Envisat operated in a sun-synchronous orbit with an equator
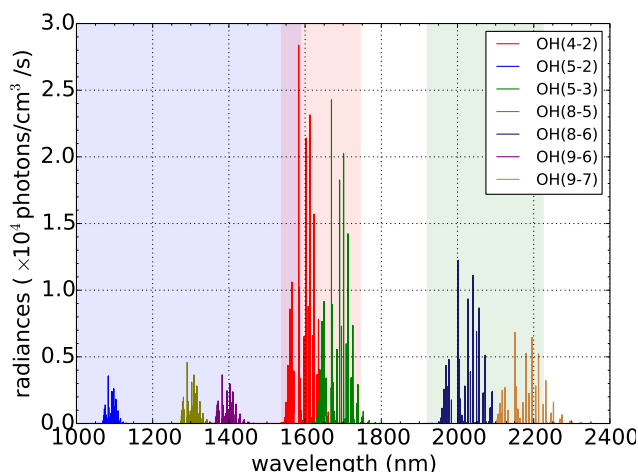
Figure 1. OH airglow emission bands used in this study in a spectral range between 1000 nm and 2400 nm. Shaded light blue region covers a spectral range observed by SCIAMACHY channel 6; shaded light red and light green regions cover two spectral ranges measured by SABER channel 9 and 8, respectively.

crossing local solar time of 10 a.m./p.m. The limb spectra used here were observed by SCIAMACHY in a dedicated meso-

55 sphere/thermosphere mode and the limb observational range covered 24 tangent altitudes from 73 km to 148 km with a vertical sampling of 3.3 km between two adjacent tangent heights. SCIAMACHY was a multi-channel grating spectrometer and its channel 6 measured OH spectra arising from vibrational states 2 to 9 at a spectral resolution of 1.5 nm. Channel 6 is considered to have been a well understood and calibrated channel, covering a spectral range from 971 nm to 1773 nm (Lichtenberg et al., 2006). In this study, only the spectral range of channel 6 up to 1650 nm was used due to the reduced performance of the detector

60 beyond this wavelength (Lichtenberg et al., 2006). It should be noted that SCIAMACHY's channel 7 and 8 covered spectral ranges of 1934-2044 nm and 2259-2386 nm, respectively, but unfortunately suffered from ice condensation on their detectors (Lichtenberg et al., 2006). The SABER, on the TIMED satellite, achieves almost 24-hour local time coverage every 60-65 days (Smith et al., 2010; Gao et al., 2010; Xu et al., 2012). SABER is a multi-channel radiometer and observes radiometric OH(9-7, 8-6) ro-vibrational lines with wavelengths around 2.0 μm by means of its channel 8 and OH(5-3, 4-2) band emissions at about

65 1.6 μm by means of its channel 9 (Xu et al., 2012). The altitude range of the observation covers 60-180 km with an altitude resolution of approx. 2 km (Mertens et al., 2009). Since the SABER instrument is a radiometer, individual OH ro-vibrational emission lines cannot be resolved. Figure 1 shows simulated OH airglow emissions in the spectral range between 1000 nm and 2400 nm; spectral ranges covered by the different instruments are shaded in different colors. As shown in Figure 1, only a small portion of the OH(4-2) band spectra is covered by both instruments.

70 Since the spectral coverage of SCIAMACHY and SABER does not coincide, we could not compare their measurements directly. However, both instruments observed ro-vibrational lines stemming from the same upper vibrational states. This offered us an opportunity to calculate the number densities of the OH upper vibrational states and then simulate the same ro-vibrational emission bands for the purposes of comparison. The SCIAMACHY channel 6 provided limb measurements of OH(4-2), OH(5-
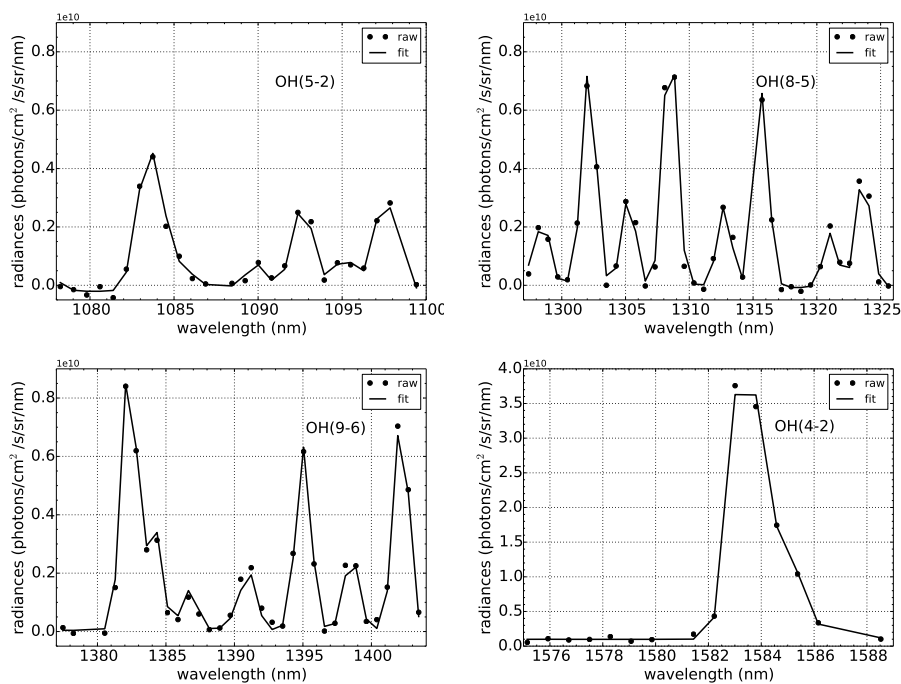
Figure 2. Monthly zonal median OH(4-2), OH(5-2), OH(8-5), and OH(9-6) limb spectra at tangent altitude about 86 km for September 2005 in a latitude range 35°N-40°N.

2), OH(8-5), and OH(9-6) band emissions, which arise from the same upper vibrational states as SABER OH radiance data. From these measurements, it was a straightforward matter to obtain the number densities of OH(v=4, 5, 8, and 9) and to simulate corresponding measurements for SABER.

In our study, OH limb spectra measured by SCIAMACHY at 1078-1100 nm, 1297-1325 nm, 1377-1404 nm, and 1575-1588 nm were used, as shown in Figure 2. The spectral ranges covered ro-vibrational lines in the OH(5-2), OH(8-5), OH(9-6) and OH(4-2) bands, respectively, with low rotational quantum numbers N ($N \leq 3$) to avoid the potential uncertainty that can be introduced by over-populated high-N rotational states (Cosby and Slanger, 2007; Noll et al., 2015; Oliva et al., 2015). The SABER V2.0 data were used in this study, including OH in-band and "unfiltered" 1.6 μm and 2.0 μm radiance measurements (Mlynczak et al., 2013). The in-band OH radiance data comprised raw data that did not take into account filter transmission, while the "unfiltered" OH radiance data used here are corrected in-band data accounting for filter characteristics measured in the lab (Xu et al., 2012). The main data used in the study consisted of "unfiltered" OH radiance data; the in-band data were not used unless otherwise stated. In order to enhance the signal-to-noise ratio and to obtain a large number of coincident measurements with both instruments, monthly zonal median data in 5-degree latitude bins were used. Since the SCIAMACHY instrument could not measure nighttime temperature in the UMLT, co-located SABER measurements were also used here. The coincidence criteria selected were ±2.5° in latitude and one hour in local time.

3 Methodology

3.1 OH emission model

The exothermic reaction of H and O_3 in the atmosphere was identified by Bates and Nicolet (1950) as the major source of vibrationally excited hydroxyl radicals (OH^*) near the mesopause region.

$$H + O_3 \rightarrow OH^*(v \leq 9) + O_2 \tag{R1}$$

Metastable excited OH^* can be de-excited via radiative, chemical, and collisional relaxation processes. $OH(v \leq 8)$ is not only initially populated by the reaction of H + O_3, but is also produced by the deactivation of higher vibrational states of OH^* via radiative relaxation and physical quenching. The number density of $OH(v)$ can be obtained from its emission measurements by dividing the corresponding Einstein coefficients. The volume emission rate $V_{v-v'}(i)$ of an arbitrary ro-vibrational line within a vibrational band $OH(v - v')$ can be calculated as

$$V_{v-v'}(i) = n_v \cdot \frac{g_v(i) \cdot e^{-E_v(i)/(k \cdot T)}}{Q_v(T)} \cdot A_{v-v'}(i) \tag{1}$$

n_v is the total number density of the corresponding upper vibrational state v and $A_{v-v'}(i)$ is the Einstein coefficient of the specific state-to-state transition from vibrational level v to v'. $E_v(i)$ and $g_v(i)$ are the rotational energy and degeneracy of the upper rotational state of the ith line considered. k is the Boltzmann factor and T is the temperature. $Q_v(T)$ is the rotational partition sum of $OH(v)$.

3.2 Retrieval model

SCIAMACHY measured integrated OH spectra along the line of sight in the tangent altitude range from approx. 73 km to approx. 149 km. If we assume that each layer emits OH airglow homogeneously, and set the retrieval grid to be identical to the tangent altitude grid of OH limb measurements, the SCIAMACHY OH limb measurements can be expressed as

$$\boldsymbol{y} = \boldsymbol{F}(\boldsymbol{x}, \boldsymbol{b}) + \boldsymbol{\epsilon} \tag{2}$$

$\boldsymbol{y}$ corresponds to the measured SCIAMACHY OH limb spectra measured. $\boldsymbol{F}$ is the functional formula of the forward model involving the equation 1. $\boldsymbol{x}$ represents the number densities (n_v) of the corresponding upper vibrational state of the emission lines. $\boldsymbol{b}$ is the parameter vector of the forward model, i.e., Einstein coefficients. $\boldsymbol{\epsilon}$ represents stochastic measurement errors. The retrieval can be regarded as an approach to solving an inverse problem in the presence of indirect measurements of interested properties. In general, the inverse problem is ill-conditioned. Therefore, an iterative non-linear regularized global fit technique introduced by Rodgers (2000) was used to solve the inverse issue.

$$\boldsymbol{x}_{i+1} = \boldsymbol{x}_a + (\boldsymbol{K}_{\boldsymbol{i}}^T \boldsymbol{S}_{\boldsymbol{\epsilon}}^{-1} \boldsymbol{K}_{\boldsymbol{i}} + \boldsymbol{S}_{\boldsymbol{a}}^{-1})^{-1} \boldsymbol{K}_{\boldsymbol{i}}^T \boldsymbol{S}_{\boldsymbol{\epsilon}}^{-1} [\boldsymbol{y} - \boldsymbol{F}(\boldsymbol{x}_i, \boldsymbol{b}) + \boldsymbol{K}_{\boldsymbol{i}}(\boldsymbol{x}_i - \boldsymbol{x}_a)] \tag{3}$$

$\boldsymbol{x}_i$ reaches the optimal estimate solution when i approaches infinity. $\boldsymbol{K}_{\boldsymbol{i}}$ corresponds to the first derivative matrix of the forward model, named the Jacobian matrix. $\boldsymbol{x}_a$ represents the a-priori knowledge of the total number densities of $OH(v)$, and $\boldsymbol{S}_{\boldsymbol{a}}$ is its diagonal error covariance matrix. $\boldsymbol{S}_{\boldsymbol{\epsilon}}$ is a diagonal error covariance matrix of $\boldsymbol{y}$.

4 Results and discussion

4.1 Error analysis

The confidence level of simulated volume emission rates (VERs) can be assessed by considering three main aspects: the uncertainty of the auxiliary atmospheric quantity, i.e., temperature; the uncertainty of the rate constant, i.e., Einstein coefficients; and the potential uncertainty introduced by over-populated high rotational states due to non-local thermodynamic equilibrium (non-LTE). The temperature uncertainty in the SABER measurements includes random and systematic errors; Dawkins et al. (2018) summarized all SABER temperature uncertainties at different altitudes for a single profile. Due to our utilization of monthly median data, only systematic errors in the SABER temperature measurements were considered in this study. The SABER systematic temperature uncertainty is approx. 1.5 K at 70-80 km. The value reaches 4 K at 90 km and 5 K at 100 km. Accordingly, VERs are affected by temperature uncertainties by less than 1% between 80 km and 96 km on average. This was also confirmed by Xu et al. (2012) in their investigation of the temperature dependence of the Einstein coefficients. They found that the OH(9-7) band Einstein coefficient only changes by approx. 0.35% when the temperature increases from 200 K to 250 K.

Many OH Einstein coefficient datasets can be found in the OH research community (Liu et al., 2015); the two latest are HITRAN molecular spectroscopic database (Gordon et al., 2017) and the OH Einstein A values calculated by Brooke et al. (2016). Figure 3 shows simulated SABER OH 1.6 μm and 2.0 μm VER profiles obtained from SCIAMACHY OH limb spectral measurements using these two Einstein datasets at 20°N-40°N for October 2007. It was found that higher VERs can be obtained using the Einstein A values calculated by Brooke et al. (2016). The differences were approx. 13% for the simulation of SABER 2.0 μm VERs and approx. 4% for the simulation of SABER 1.6 μm VERs. Similar values were also obtained if we used data from other latitude bins or time periods. Therefore, we used these results as a proxy to estimate related uncertainties, which are in the range of 4% and 13% for simulations of OH 1.6 μm and 2.0 μm VERs.

It was observed that high rotational states ($N \geq 4$) of OH do not meet the LTE hypothesis and that these levels are over-populated (Cosby and Slanger, 2007; Noll et al., 2015; Oliva et al., 2015). It is difficult to estimate the non-LTE-induced overpopulation of high OH rotational states using SCIAMACHY data due to its low spectral resolution, which results in an overlap of emission lines arising from low and high OH upper rotational states. An estimation of the non-LTE contribution was performed by Oliva et al. (2015) based on cross-dispersed cryogenic spectrometer measurements in the spectral range of 0.97 μm to 2.4 μm. A combination of two Boltzmann distribution equations with cold and hot OH rotational temperatures was used to predict the observed intensities of OH emission lines. Kalogerakis et al. (2018) re-analyzed the data used by Oliva et al. (2015) to estimate the OH rotational temperatures following the approach taken by Cosby and Slanger (2007) and Oliva et al. (2015). They found that the thermalization of every OH vibrational level is incomplete. In our study, we used the same methods and parameters (cold and hot temperatures) determined by Oliva et al. (2015) and Kalogerakis et al. (2018) to estimate the VER uncertainty introduced by the non-LTE effect, and found that the contribution is less than 2% for both SABER channels.

In summary, the uncertainty of the Einstein coefficient dominates the error budget, which is in the order of 5% and 14% for the SABER 1.6 μm and 2.0 μm VER simulations, respectively.
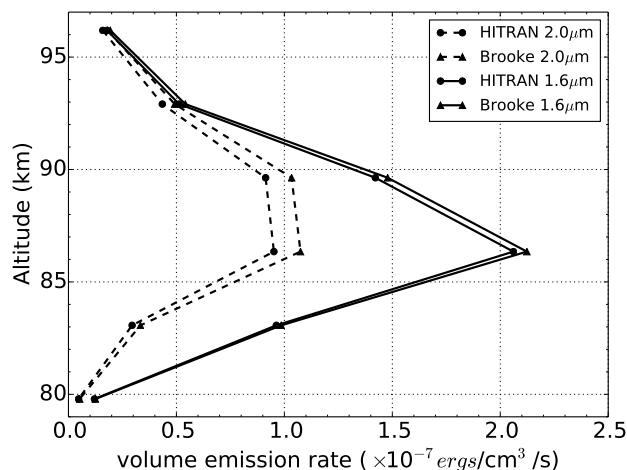
Figure 3. Simulated SABER OH 1.6 μm and 2.0 μm volume emission rates from SCIAMACHY data using Einstein A values of HITRAN and Brooke et al. (2016) at 20°N-40°N for October 2007.

4.2 Comparison of SABER measurements and simulations

SABER OH 1.6 μm and 2.0 μm VERs were simulated using SCIAMACHY OH nighttime limb spectra based on HITRAN OH
155 Einstein A values. Two examples of the intercomparison between SABER measurements and simulations are given in Figure 4 for September 2005 at latitude bins 0°-20°N (left) and 20°N-40°N (right). It was found that measured VERs are always larger than the simulations using SCIAMACHY data. Deviations between SABER OH 1.6 μm measurements and the corresponding simulations increase with altitude from approx. 20% (36%) at 83 km to approx. 49% (74%) at 96 km in the latitude range 0°-20°N (20°N-40°N). The difference between SABER OH 2.0 μm measurements and the corresponding simulations is approx.
160 15% at 86 km. At approx. 96 km, it reaches approx. 64% in latitude bins 0°-20°N and approx. 88% in 20°N-40°N. Large relative deviations between the measurements and simulations were found above OH emission peak altitudes. It was also found the positive deviations of SABER in-band data from the simulated values, especially for OH 2.0 μm data.

Figure 5 shows the global spatial distributions of SABER OH 2.0 μm VERs (bottom) and the corresponding simulations (top) using SCIAMACHY data from the year 2007. The two datasets show the same OH radiative spatial structures from a
165 global perspective. A strong annual oscillation was found over the equator region in April and OH emission data show a peak at approx. 87 km. This indicates that the two instruments (SCIAMACHY and SABER) successfully captured the same dynamical features. It is clear that SABER VERs are significantly larger than corresponding simulated values based on SCIAMACHY observations, especially at VER peak altitudes. Comparing the SABER OH 1.6 μm VERs and the corresponding simulations leads to the same conclusion (not shown here).

170 A correlation diagram is a common means to visualize and quantify the interdependency of two datasets. Figure 6 shows two scatter plots which elucidate the consistency of SABER 1.6 μm (left) and 2.0 μm (right) VERs and corresponding simulated values based on SCIAMACHY observations for the year 2007. In general, SABER OH data show larger radiance values
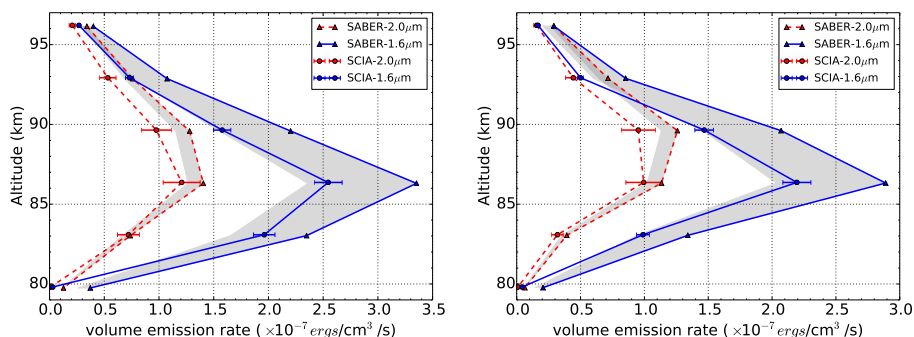
Figure 4. SABER 1.6 μm and 2.0 μm volume emission rates and corresponding simulations from SCIAMACHY data for September 2005 at latitude bins 0°-20°N (left) and 20°N-40°N (right). The horizontal lines represent error bars considering the uncertainties of the Einstein coefficient and the SABER temperature. The lower and upper bounds of grey shaded area indicate SABER in-band and "unfiltered" OH radiance data, respectively.

compared to the simulations using SCIAMACHY data, and there is a clear linear relationship between them. To obtain a rough estimate of the ratio between SABER data and the corresponding simulations, a straightforward linear fit was performed. For

175   OH 1.6 μm radiances, the ratio of SABER versus SCIAMACHY data is 1.24. For OH 2.0 μm data, the ratio is approx. 1.04, as shown in Figure 6.

Figure 7 shows the ratio of SABER data to the corresponding simulations based on SCIAMACHY data from 2003 to 2011. For the OH 1.6 μm data, the ratio value varies roughly between 1.2 and 1.3 for 2003-2009, reaching 1.1 for 2010 and 1.36 for 2011. The ratio varies between 1.0 and 1.1 for the OH 2.0 μm data. The data indicate that there are no significant variations

180   in the slope of SABER data versus SCIAMACHY simulations from 2003 to 2011 and that there is a systematic bias between them in general.

5   Conclusions

Near-infrared OH nightglow emissions measured by SCIAMACHY channel 6 were used in this study to simulate SABER 1.6 μm and 2.0 μm radiance measurements. The Einstein coefficients were the main source of uncertainty, leading to uncertainties in the order of 13% for the OH 2.0 μm radiance simulation and 4% for the OH 1.6 μm radiance simulation. Both instruments

185   captured the spatial structures of OH volume emission rates. The ratio of SABER OH 1.6 μm (2.0 μm) radiance measurements to the simulations based on SCIAMACHY data varied in the range of 1.2-1.4 (1.0-1.1) from 2003 to 2011. The differences between the SCIAMACHY and SABER OH radiance measurements may be explained by the radiometric calibration of the two instruments.
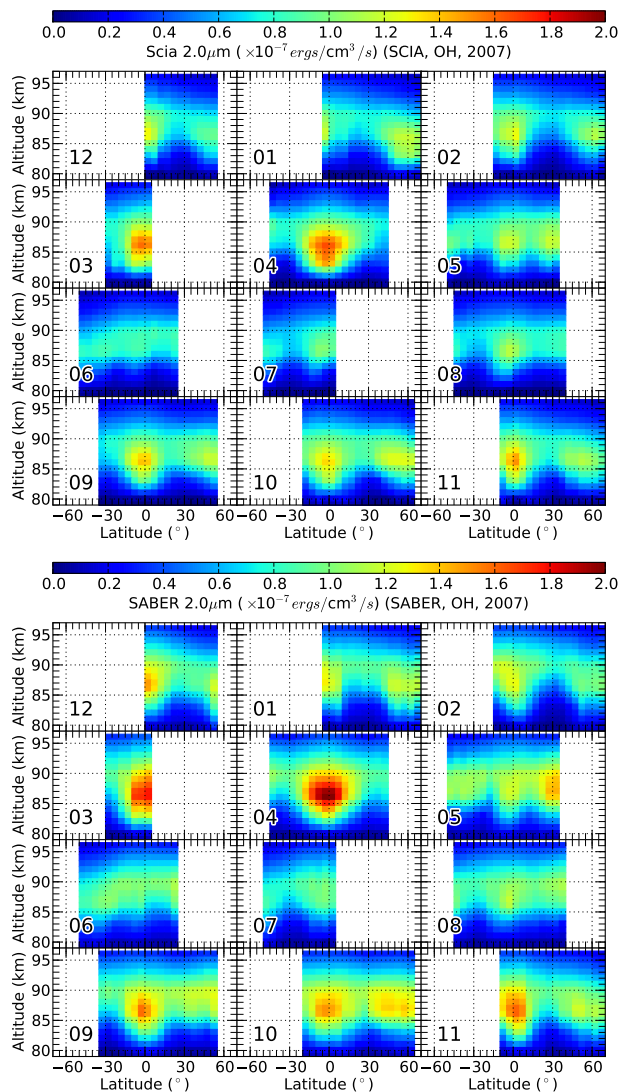
Figure 5. Latitude-altitude cross sections of monthly zonal median SABER 2.0 μm volume emission rates (bottom) and corresponding simulations (top) from SCIAMACHY data for the year 2007. The numbers represent the month of the year.

Data availability. The SCIAMACHY Level 1b Version 8 data used in this study are available at ftp://scia-ftp-ds.eo.esa.int. SABER Version 2.0 data are available at http://saber.gats-inc.com. Derived OH volume emission rate data are available on request.

Competing interests. The authors declare that they have no conflict of interest.
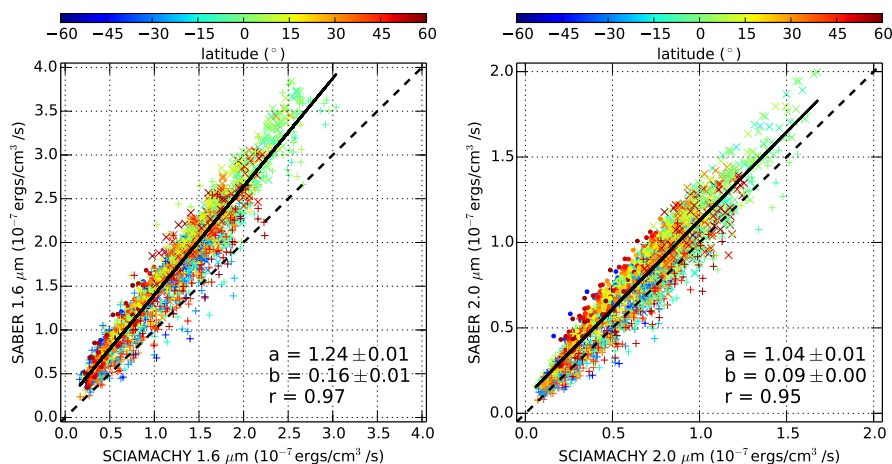
Figure 6. Scatter plots of SABER 1.6 μm (left) and 2.0 μm (right) volume emission rates versus the corresponding simulations using SCIAMACHY data for the year 2007. The color bar shows the latitude. The plus marker indicates the data at 80-85 km, the x marker represents the data at 86-90 km, and the point marker shows the data at 91-95 km. The solid line shows the linear fit to the data. a and b represent the slope and y-intercept of the fitting line, respectively. r represents the correlation coefficient of the fitting.
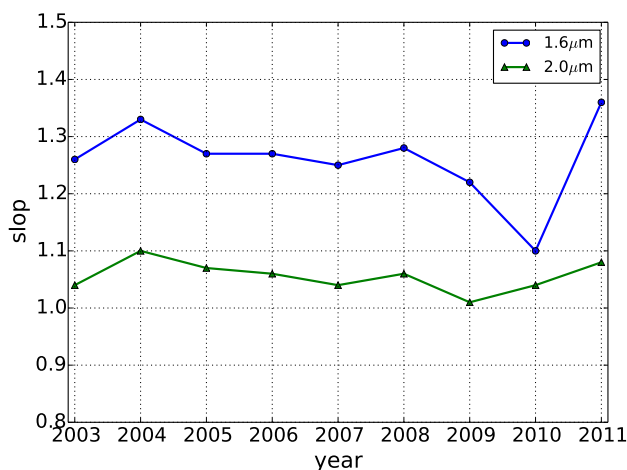
Figure 7. Slops of SABER 2.0 μm and 1.6 μm volume emission rates versus the corresponding simulations using SCIAMACHY data from 2003 to 2011.

Acknowledgements. The work of Y. Zhu was supported by the 2017 Helmholtz-OCPC-Programme and the International Postdoctoral Exchange Fellowship Program 2017. Q. Chen, Q. Gong, J. Liu, and D. Wei were supported in their work by the China Scholarship Council. M. Kaufmann was supported by Forschungszentrum Jülich.

195

References

Baker, D. J. and Stair, A. T. J.: Rocket measurements of the altitude distributions of the hydroxyl airglow, Physica Scripta, 37, 611, http://stacks.iop.org/1402-4896/37/i=4/a=021, 1988.

Bates, D. R. and Nicolet, M.: The photochemistry of atmospheric water vapor, Journal of Geophysical Research, 55, 301–327, https://doi.org/10.1029/JZ055i003p00301, http://dx.doi.org/10.1029/JZ055i003p00301, 1950.

Brooke, J. S., Bernath, P. F., Western, C. M., Sneden, C., Afşar, M., Li, G., and Gordon, I. E.: Line strengths of rovibrational and rotational transitions in the $X^2\Pi$ ground state of OH, Journal of Quantitative Spectroscopy and Radiative Transfer, 168, 142 – 157, https://doi.org/https://doi.org/10.1016/j.jqsrt.2015.07.021, http://www.sciencedirect.com/science/article/pii/S0022407315002721, 2016.

Cosby, P. C. and Slanger, T. G.: OH spectroscopy and chemistry investigated with astronomical sky spectra, Canadian Journal of Physics, 85, 77–99, https://doi.org/10.1139/p06-088, http://www.nrcresearchpress.com/doi/abs/10.1139/p06-088, 2007.

Dawkins, E. C. M., Feofilov, A., Rezac, L., Kutepov, A. A., Janches, D., Höffner, J., Chu, X., Lu, X., Mlynczak, M. G., and Russell III, J.: Validation of SABER v2.0 Operational Temperature Data With Ground-Based Lidars in the Mesosphere-Lower Thermosphere Region (75 - 105 km), Journal of Geophysical Research: Atmospheres, 123, 9916–9934, https://doi.org/10.1029/2018JD028742, https://agupubs.onlinelibrary.wiley.com/doi/abs/10.1029/2018JD028742, 2018.

Gao, H., Xu, J., and Wu, Q.: Seasonal and QBO variations in the OH nightglow emission observed by TIMED/SABER, Journal of Geophysical Research: Space Physics, 115, n/a–n/a, https://doi.org/10.1029/2009JA014641, http://dx.doi.org/10.1029/2009JA014641, a06313, 2010.

Gordon, I., Rothman, L., Hill, C., Kochanov, R., Tan, Y., Bernath, P., Birk, M., Boudon, V., Campargue, A., Chance, K., Drouin, B., Flaud, J.-M., Gamache, R., Hodges, J., Jacquemart, D., Perevalov, V., Perrin, A., Shine, K., Smith, M.-A., Tennyson, J., Toon, G., Tran, H., Tyuterev, V., Barbe, A., Császár, A., Devi, V., Furtenbacher, T., Harrison, J., Hartmann, J.-M., Jolly, A., Johnson, T., Karman, T., Kleiner, I., Kyuberis, A., Loos, J., Lyulin, O., Massie, S., Mikhailenko, S., Moazzen-Ahmadi, N., Müller, H., Naumenko, O., Nikitin, A., Polyansky, O., Rey, M., Rotger, M., Sharpe, S., Sung, K., Starikova, E., Tashkun, S., Auwera, J. V., Wagner, G., Wilzewski, J., Wcisło, P., Yu, S., and Zak, E.: The HITRAN2016 molecular spectroscopic database, Journal of Quantitative Spectroscopy and Radiative Transfer, 203, 3 – 69, https://doi.org/https://doi.org/10.1016/j.jqsrt.2017.06.038, http://www.sciencedirect.com/science/article/pii/S0022407317301073, HITRAN2016 Special Issue, 2017.

Kalogerakis, K. S., Matsiev, D., Sharma, R. D., and Wintersteiner, P. P.: Resolving the mesospheric nighttime 4.3 μm emission puzzle: Laboratory demonstration of new mechanism for OH(ν) relaxation, Geophysical Research Letters, 43, 8835–8843, https://doi.org/10.1002/2016GL069645, https://agupubs.onlinelibrary.wiley.com/doi/abs/10.1002/2016GL069645, 2016.

Kalogerakis, K. S., Matsiev, D., Cosby, P. C., Dodd, J. A., Falcinelli, S., Hedin, J., Kutepov, A. A., Noll, S., Panka, P. A., Romanescu, C., and Thiebaud, J. E.: New insights for mesospheric OH: multi-quantum vibrational relaxation as a driver for non-local thermodynamic equilibrium, Annales Geophysicae, 36, 13–24, https://doi.org/10.5194/angeo-36-13-2018, https://www.ann-geophys.net/36/13/2018/, 2018.

Kaufmann, M., Lehmann, C., Hoffmann, L., Funke, B., López-Puertas, M., Savigny, C., and Riese, M.: Chemical heating rates derived from SCIAMACHY vibrationally excited OH limb emission spectra, Advances in Space Research, 41, 1914 – 1920, https://doi.org/http://dx.doi.org/10.1016/j.asr.2007.07.045, http://www.sciencedirect.com/science/article/pii/S0273117707008459, 2008.

Kaufmann, M., Ern, M., Lehmann, C., and Riese, M.: The Response of Atomic Hydrogen to Solar Radiation Changes, in: Climate and Weather of the Sun-Earth System (CAWSES), edited by Lübken, F.-J., Springer Atmospheric Sciences, pp. 171–188, Springer Netherlands, http://dx.doi.org/10.1007/978-94-007-4348-9_10, 2013.

Kaufmann, M., Zhu, Y., Ern, M., and Riese, M.: Global distribution of atomic oxygen in the mesopause region as derived from SCIAMACHY O(^{1}S) green line measurements, Geophysical Research Letters, 41, 6274–6280, https://doi.org/10.1002/2014GL060574, http://dx.doi.org/10.1002/2014GL060574, 2014.

Lichtenberg, G., Kleipool, Q., Krijger, J. M., van Soest, G., van Hees, R., Tilstra, L. G., Acarreta, J. R., Aben, I., Ahlers, B., Bovensmann, H., Chance, K., Gloudemans, A. M. S., Hoogeveen, R. W. M., Jongma, R. T. N., Noël, S., Piters, A., Schrijver, H., Schrijvers, C., Sioris, C. E., Skupin, J., Slijkhuis, S., Stammes, P., and Wuttke, M.: SCIAMACHY Level 1 data: calibration concept and in-flight calibration, Atmospheric Chemistry and Physics, 6, 5347–5367, https://doi.org/10.5194/acp-6-5347-2006, https://www.atmos-chem-phys.net/6/5347/2006/, 2006.

Liu, W., Xu, J., Smith, A. K., and Yuan, W.: Comparison of rotational temperature derived from ground-based OH airglow observations with TIMED/SABER to evaluate the Einstein coefficients, Journal of Geophysical Research: Space Physics, 120, 10 069–10 082, https://doi.org/10.1002/2015JA021886, http://dx.doi.org/10.1002/2015JA021886, 2015JA021886, 2015.

Meinel, I. A. B.: OH Emission Bands in the Spectrum of the Night Sky, Astrophys. J., 111, 555–564, 1950.

Mertens, C. J., III, J. M. R., Mlynczak, M. G., She, C.-Y., Schmidlin, F. J., Goldberg, R. A., López-Puertas, M., Wintersteiner, P. P., Picard, R. H., Winick, J. R., and Xu, X.: Kinetic temperature and carbon dioxide from broadband infrared limb emission measurements taken from the TIMED/SABER instrument, Advances in Space Research, 43, 15 – 27, https://doi.org/https://doi.org/10.1016/j.asr.2008.04.017, http://www.sciencedirect.com/science/article/pii/S0273117708002883, 2009.

Mlynczak, M. G., Hunt, L. A., Thomas Marshall, B., Martin-Torres, F. J., Mertens, C. J., Russell, J. M., Remsberg, E. E., López-Puertas, M., Picard, R., Winick, J., Wintersteiner, P., Thompson, R. E., and Gordley, L. L.: Observations of infrared radiative cooling in the thermosphere on daily to multiyear timescales from the TIMED/SABER instrument, Journal of Geophysical Research: Space Physics, 115, n/a–n/a, https://doi.org/10.1029/2009JA014713, http://dx.doi.org/10.1029/2009JA014713, a03309, 2010.

Mlynczak, M. G., Hunt, L. A., Mast, J. C., Thomas Marshall, B., Russell, J. M., Smith, A. K., Siskind, D. E., Yee, J.-H., Mertens, C. J., Javier Martin-Torres, F., Earl Thompson, R., Drob, D. P., and Gordley, L. L.: Atomic oxygen in the mesosphere and lower thermosphere derived from SABER: Algorithm theoretical basis and measurement uncertainty, Journal of Geophysical Research: Atmospheres, 118, 5724–5735, https://doi.org/10.1002/jgrd.50401, http://doi.wiley.com/10.1002/jgrd.50401, 2013.

Mlynczak, M. G., A., H. L., Russell III, J. M., and Marshall, B. T.: Updated SABER Night Atomic Oxygen and Implications for SABER Ozone and Atomic Hydrogen, Geophysical Research Letters, 45, 5735–5741, 2018.

Noll, S., Kausch, W., Kimeswenger, S., Unterguggenberger, S., and Jones, A. M.: OH populations and temperatures from simultaneous spectroscopic observations of 25 bands, Atmospheric Chemistry and Physics, 15, 3647–3669, https://doi.org/10.5194/acp-15-3647-2015, http://www.atmos-chem-phys.net/15/3647/2015/, 2015.

Offermann, D. and Gerndt, R.: Upper mesosphere temperatures from OH*-emissions, Advances in Space Research, 10, 217 – 221, https://doi.org/http://dx.doi.org/10.1016/0273-1177(90)90399-K, http://www.sciencedirect.com/science/article/pii/027311779090399K, 1990.

Offermann, D., Hoffmann, P., Knieling, P., Koppmann, R., Oberheide, J., and Steinbrecht, W.: Long-term trends and solar cycle variations of mesospheric temperature and dynamics, Journal of Geophysical Research: Atmospheres, 115, n/a–n/a, https://doi.org/10.1029/2009JD013363, http://dx.doi.org/10.1029/2009JD013363, d18127, 2010.

Oliva, E., Origlia, L., Scuderi, S., Benatti, S., Carleo, I., Lapenna, E., Mucciarelli, A., Baffa, C., Biliotti, V., Carbonaro, L., Falcini, G., Giani, E., Iuzzolino, M., Massi, F., Sanna, N., Sozzi, M., Tozzi, A., Ghedina, A., Ghinassi, F., Lodi, M., Harutyunyan, A., and Pedani, M.: Lines and continuum sky emission in the near infrared: observational constraints from deep high spectral resolution spectra with

GIANO-TNG, Astronomy&Atrophysics, 581, A47, https://doi.org/10.1051/0004-6361/201526291, https://doi.org/10.1051/0004-6361/201526291, 2015.

Panka, P. A., Kutepov, A. A., Rezac, L., Kalogerakis, K. S., Feofilov, A. G., Marsh, D., Janches, D., and Yiğit, E.: Atomic Oxygen Retrieved From the SABER 2.0- and 1.6-μm Radiances Using New First-Principles Nighttime OH(v) Model, Geophysical Research Letters, 45,
275   5798–5803, https://doi.org/10.1029/2018GL077677, https://agupubs.onlinelibrary.wiley.com/doi/abs/10.1029/2018GL077677, 2018.

Rodgers, C. D.: Inverse Methods for Atmospheric Sounding: Theory and Practice, vol. 2 of *Series on Atmospheric, Oceanic and Planetary Physics*, World Scientific, Singapore, 2000.

Smith, A. K., Marsh, D. R., Russell, J. M., Mlynczak, M. G., Martin-Torres, F. J., and Kyrölä, E.: Satellite observations of high nighttime ozone at the equatorial mesopause, Journal of Geophysical Research, 113, https://doi.org/10.1029/2008JD010066, http://doi.wiley.com/
280   10.1029/2008JD010066, 2008.

Smith, A. K., Marsh, D. R., Mlynczak, M. G., and Mast, J. C.: Temporal variations of atomic oxygen in the upper mesosphere from SABER, Journal of Geophysical Research, 115, https://doi.org/10.1029/2009JD013434, http://doi.wiley.com/10.1029/2009JD013434, 2010.

von Savigny, C., Eichmann, K.-U., Llewellyn, E. J., Bovensmann, H., Burrows, J. P., Bittner, M., Höppner, K., Offermann, D., Taylor, M. J., Zhao, Y., Steinbrecht, W., and Winkler, P.: First near-global retrievals of OH rotational temperatures from satellite-based Meinel band
285   emission measurements, Geophysical Research Letters, 31, n/a–n/a, https://doi.org/10.1029/2004GL020410, http://dx.doi.org/10.1029/2004GL020410, l15111, 2004.

von Savigny, C., McDade, I. C., Eichmann, K.-U., and Burrows, J. P.: On the dependence of the OH* Meinel emission altitude on vibrational level: SCIAMACHY observations and model simulations, Atmospheric Chemistry and Physics, 12, 8813–8828, https://doi.org/10.5194/acp-12-8813-2012, http://www.atmos-chem-phys.net/12/8813/2012/, 2012.

290   Xu, J., Smith, A. K., Yuan, W., Liu, H.-L., Wu, Q., Mlynczak, M. G., and Russell, J. M.: Global structure and long-term variations of zonal mean temperature observed by TIMED/SABER, Journal of Geophysical Research: Atmospheres, 112, https://doi.org/10.1029/2007JD008546, http://dx.doi.org/10.1029/2007JD008546, 2007.

Xu, J., Gao, H., Smith, A. K., and Zhu, Y.: Using TIMED/SABER nightglow observations to investigate hydroxyl emission mechanisms in the mesopause region, Journal of Geophysical Research: Atmospheres, 117, n/a–n/a, https://doi.org/10.1029/2011JD016342, http://dx.
295   doi.org/10.1029/2011JD016342, 2012.

Xu, J., Li, Q., Yue, J., Hoffmann, L., Straka, W. C., Wang, C., Liu, M., Yuan, W., Han, S., Miller, S. D., Sun, L., Liu, X., Liu, W., Yang, J., and Ning, B.: Concentric gravity waves over northern China observed by an airglow imager network and satellites, Journal of Geophysical Research: Atmospheres, 120, 11,058–11,078, https://doi.org/10.1002/2015JD023786, http://dx.doi.org/10.1002/2015JD023786, 2015JD023786, 2015.

300   Zhu, Y. and Kaufmann, M.: Atomic oxygen abundance retrieved from SCIAMACHY hydroxyl nightglow measurements, Geophysical Research Letters, 45, 9314–9322, https://doi.org/10.1029/2018GL079259, https://agupubs.onlinelibrary.wiley.com/doi/abs/10.1029/2018GL079259, 2018.

Zhu, Y. and Kaufmann, M.: Consistent Nighttime Atomic Oxygen Concentrations from O_2 A-band, $O(^1S)$ Green-Line, and OH Airglow Measurements as Performed by SCIAMACHY, Geophysical Research Letters, 46, 8536–8545, https://doi.org/10.1029/2019GL083550,
305   https://agupubs.onlinelibrary.wiley.com/doi/abs/10.1029/2019GL083550, 2019.

Zhu, Y., Xu, J., Yuan, W., and Liu, X.: First experiment of spectrometric observation of hydroxyl emission and rotational temperature in the mesopause in China, Science China Technological Sciences, 55, 1312–1318, https://doi.org/10.1007/s11431-012-4824-7, http://dx.doi.org/10.1007/s11431-012-4824-7, 2012.

Zhu, Y., Kaufmann, M., Ern, M., and Riese, M.: Nighttime atomic oxygen in the mesopause region retrieved from SCIAMACHY O(^{1}S)
310   green line measurements and its response to solar cycle variation, Journal of Geophysical Research: Space Physics, 120, 9057–9073,
https://doi.org/10.1002/2015JA021405, http://dx.doi.org/10.1002/2015JA021405, 2015.